Nouvelle forme d'onde et récepteur avancé pour la télémesure des futurs lanceurs

Charles-Ugo Piat-Durozoi

INPT: C. Poulliat, N. Thomas, M.-L. Boucheret

CNES: E. Bouisson and G. Lesthievent

charles-ugo.piat@tesa.prd.fr

Thesis Defense, November 27, 2018

Table of Content

Table of Content

Context

- Communication link launcher/ground stations
- Launcher Telemetry System (TM)
  - Position (GPS inertial system), Velocity, Video...
  - Rate $\sim$ 1Mbs
  - S-band

Open issues on the TM communication link

- Issues occurring during the rocket flight :
  - Disturbed channel (non-coherent)
    - Vibration spreading over the launcher
    - Flame Effects
- Impact on the signal :
  - Phase shift/Phase hopping
- Impact on the system performances
  - Rate losses/Total loss of the communication link
- Solution :
  - Robust modulation methods
    - Continuous Phase Modulations (CPMs)
  - Adequate detector
  - Efficient coding and precoding methods

Contributions

- Novel non-coherent symbol/MAP receiver.
- Design of precoding enabling efficient decoding.
- Optimization of capacity-achieving codes.

Table of Content

System Model

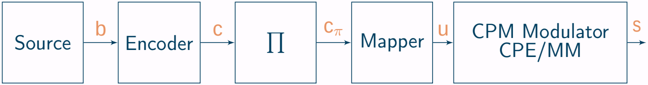

Figure: BICM block diagram

- $\mathrm{b} \in GF(2)^{K_b}$ is encoded into a codeword $\mathrm{c} \in GF(2)^{N_b}$ using an ECC of rate $R = K_b/N_b$.
- c is interleaved, mapped into a sequence $\mathrm{u} = u_0^{N_s-1}$ of N_s M-ary symbols.
- u is modulated into $\mathrm{s} = s_{L-1}^{N_s-1}(t)$ comprises of M_s distinct waveforms following the considered CPM rule.

Continuous Phase Modulation

- Signal s has a constant envelope and a continuous phase. [AAS13][Pro]

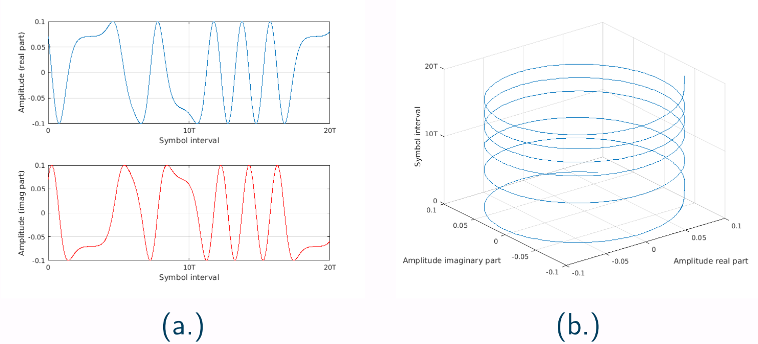

Figure: Binary 2GMSK $h = 1/2$, $BT = 0.25$ (a.) Amplitude (b.) Envelop.

Continuous Phase Modulation

- Its Rimoldi's representation at the k^{th} symbol interval is given as:

$$s_k(\tau) = \sqrt{Es} \cdot x_i(\tau) \cdot e^{j\phi_k} \quad (1)$$

- The CPE ensures the phase continuity by accumulating the phase of each symbol.

$$\phi_{k+1} = \phi_k + 2\pi h u_{k-L+1} \quad (2)$$

- The MM maps the L symbols in memory to a continuous-time waveform.

$$x_i(\tau) = \frac{A(\tau)}{\sqrt{T}} \cdot e^{j4\pi h \sum_{n=0}^{L-1} u_{k-n} q(\tau+nT)} \quad (3)$$

Continuous Phase Modulation

- $A(\tau)$ is the Rimoldi representation's data independent terms.

$$A(\tau) = e^{j\pi h(M-1)\left(\frac{\tau}{T}+(L-1)-2\sum_{n=0}^{L-1} q(\tau+nT)\right)} \quad (4)$$

- Index i is given as follows.

$$i = \sum_{n=0}^{L-1} u_{k-n} \cdot M^{L-1-n} \quad (5)$$

Continuous Phase Modulation

- In expression (1),(2),(3), elements are identified as follows:
  - T the symbol period.
  - Es the energy per symbol.
  - L the memory of the CPM.
  - h the modulation index.
  - $q(t)$ the phase response.

$$q(t) = \begin{cases} 0, & t \leq 0 \\ \int_0^t g(u)du, & 0 < t \leq LT \\ \frac{1}{2}, & t > LT \end{cases} \quad (6)$$

  - $g(u)$ the frequency pulse.

Frequency pulse and Phase response

- Differentiate the various types of CPMs
- Frequency pulse
  - GMSK : Gaussian Pulse
  - RC : Raise Cosine Pulse
  - REC : Rectangular pulse (CPFSK : REC $L = 1$)

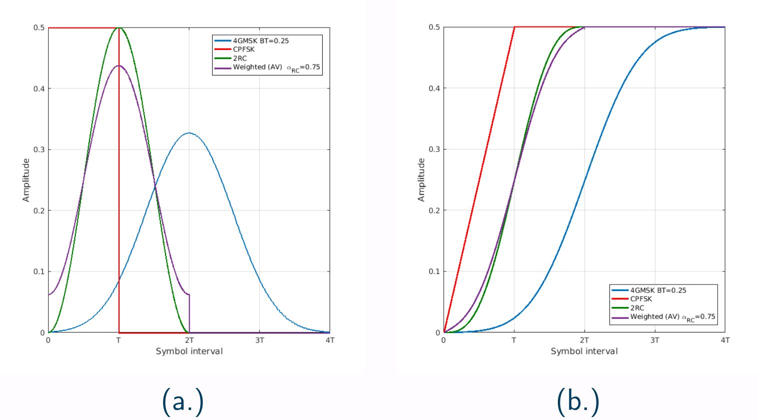

Figure: (a.) Frequency pulse (b.) Phase response.

Modulation index h and CPM memory L

- Modulation index h
  - Rational number
  - $h < 1$
  - $h = P/Q$, where P and Q are relatively prime
  - Q cardinality of the set of CPM accumulated phases
- CPM memory L
  - Full response CPM: $L = 1$
  - Partial response CPM: $L > 1$
  - Large L generates large complexity

Impact of H and L on the signal spectrum

- Modulation index h
  - Small values of h generate small bandwidth occupancy.
- CPM memory L
  - Large values of L generate small bandwidth occupancy and small side lobes sizes.

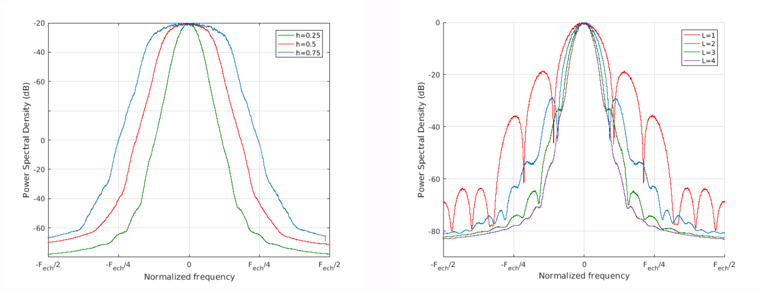

(a.) (b.)

Figure: RC (a.) quaternary $L = 3$ (b.) binary $h = 0.5$

Channel Modelization

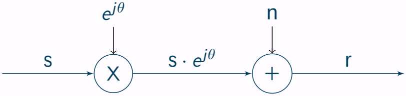

Figure: Channel model

- The signal undergoes a phase rotation θ and is passed through an AWGN channel. At the k^{th} symbol interval,

$$r_k(t) = s_k(t) \cdot e^{j\theta} + n(t) \tag{7}$$

Here $\mathbf{r} = r_{L-1}^{N_s-1}$, θ is unknown, constant over a frame and uniformly distributed between $[0, 2\pi[$.

Matched filters

- Sufficient statistics: $r_k(t)$ is passed through a bank of M_s matched filters:

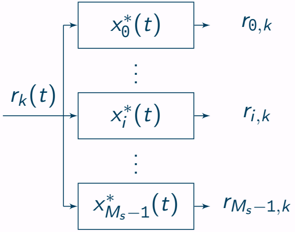

Figure: Complex matched filters for a given modulation

- $r_{i,k}$ results from the correlation between $r_k(t)$ and $x_i^*(t)$:

$$r_{i,k} = \int_0^T r_k(t) x_i^*(t) dt \tag{8}$$

Notation: $r_k = \{r_{L-1,k}, \ldots, r_{M_s-1,k}\}$

Detection process

- Coherent detection [Rim88]
  - θ is known
  - Optimal detection: Trellis-based algorithm
  - BCJR/Viterbi
  - Criteria MAP/ML
- Non-coherent detection
  - θ is unknown
  - Receiver:
    - Trellis-based algorithm (BCJR/Viterbi, MAP/ML, [CFR00],[DS90])
    - Block-based algorithm ([RD99],[VCT10])

Finite length simulation

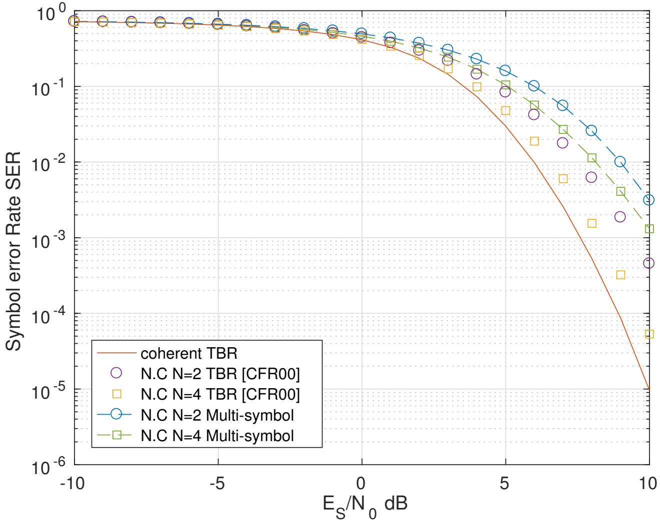

Figure: SER: CPFSK $L = 1$, $M = 4$, $h = 5/7$

Asymptotic simulation

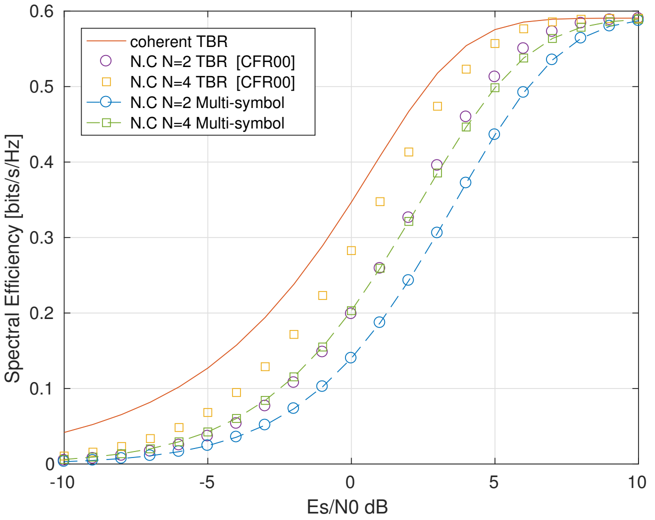

Figure: Spectral E□ciency: CPFSK $L = 1$, $M = 4$, $h = 5/7$

Table of Content

MAP versus ML

Ref.	[CFR00]	[DS90]
Algorithm	BCJR	Viterbi
Criteria	MAP	ML
States	$\{\phi, u_{k-G}, \dots, u_{k-1}\}$	$\{u_{k-G}, \dots, u_{k-1}\}$
State Space	Extended	Reduced

Table: Comparison MAP vs ML detection.

- The two references for the non-coherent detection ([CFR00],[DS90]) give equivalent performances.
- The ML returns the most likely sequence.
- The MAP maximizes the probability of each symbol.

$$\begin{aligned} \hat{u}_{ML,k} &= \arg\max_{u_0^{N_s-1}} \{p(r_{L-1}^{N_s-1} | u_0^{N_s-1})\} \\ \hat{u}_{MAP,k} &= \arg\max_{u_k} \{p(u_k | r_{L-1}^{N_s-1})\} \end{aligned} \tag{9}$$

Line of thought

- Perform soft detection
- Implement ref. [CFR00]
- Strong complexity
- Looking for complexity reduction
- Ref. [DS90] implemented ML detection with reduced state space
- Derive MAP equations with the reduced state space
- Implement and simulate the MAP detector based on both state space
  - Asymptotic simulation
  - Finite length simulation

Exit charts analysis

- Mutual information between X and $\mathcal{L}$ [Hag04]:

$$I(X,\mathcal{L}) = \frac{1}{2} \sum_{x=-1,1} \int_{-\infty}^{+\infty} p(l|X=x) \cdot log_2 \left(\frac{2p(l|X=x)}{p(l|X=-1)+p(l|X=1)} \right) dl \quad (10)$$

- *A priori* information $I_a = I(X,\mathcal{L}_a)$ ([TB01]).
- *Extrinsic* information $I_e = I(X,\mathcal{L}_e)$.
- EXIT chart: plot I_e vs I_a.

Exit charts analysis

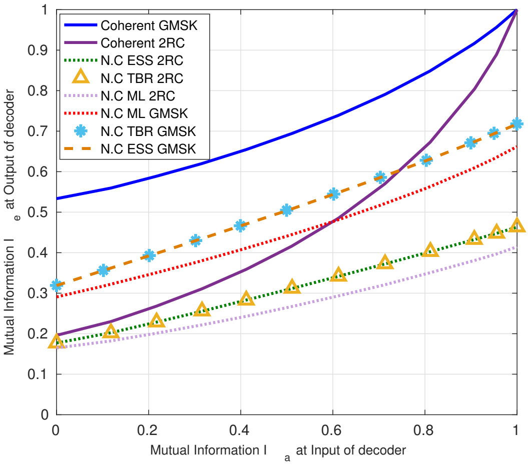

Figure: EXIT charts: 2GMSK $h = 1/2$, $M = 2$ and $BT = 0.25$ and 2RC with $h = 1/4$, $M = 4$ ($N = 3$)

Asymptotic simulation

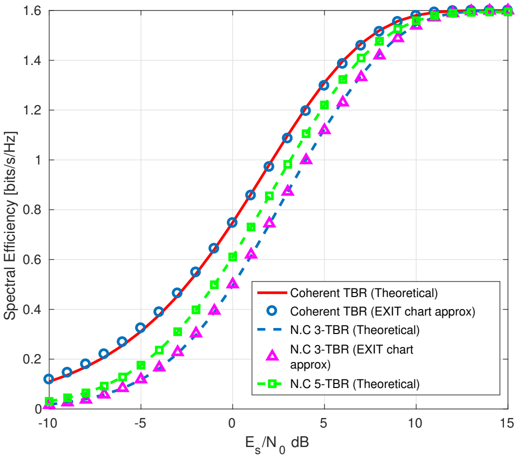

Figure: Spectral E□ciency: quaternary 2RC with $h = 1/4$.

Finite length simulation

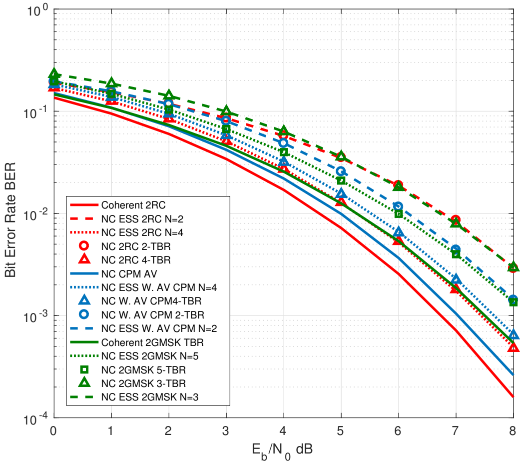

Figure: BER: 2GMSK with $h = 1/2$, $M = 2$, $BT = 0.25$, Weigthed AV CPM [SG13] $h = 1/3$, $M = 4$, 2RC $h = 1/3$, $M = 4$. ($N = 3$)

Outcome

- Taking into account the accumulated phase in the non-coherent state space can be shown to be useless
  - no information gain
  - Higher complexity
  - The reduced state space can be shown minimal

On the link between MAP and ML equations

- The metrics of the novel Non-coherent TBR:

$$\begin{cases} \gamma(\delta_k \rightarrow \delta_{k+1}, r_{k-N+1}^{k}) = \frac{1}{Q} \cdot \sum_{\{\phi_{k-N+1}\}} \gamma(\delta'_k \rightarrow \delta'_{k+1}, r_{k-N+1}^{k}) \\ \alpha_k(\delta_k) = \sum_{\{\phi_{k-N+1}\}} \alpha(\delta'_k) \\ \beta_k(\delta_k) = \frac{1}{Q} \cdot \sum_{\{\phi_{k-N+1}\}} \beta_k(\delta'_k) \end{cases} \quad (11)$$

Contributions

- Complexity reduction:
  - [CFR00] approach : $\mathcal{O}(8(N+Q)M^{N+L-1})$.
  - Novel approach : $\mathcal{O}(8NM^{N+L-1})$.
- Phase information is unknown in non-coherent regime
- The Extended State Space is a good tool to study, in the meantime, both regimes.

Journal Paper : *Piat-Durozoi, C. U.*, Poulliat, C., Boucheret, M. L., Thomas, N., Bouisson, E., & Lesthievent, G. Minimal state non-coherent symbol MAP detection of Continuous-Phase-Modulations. IEEE Communication Letter, 2018.

Journal Paper : *Piat-Durozoi, C. U.*, Poulliat, C., Boucheret, M. L., Thomas, N., Bouisson, E., & Lesthievent, G. On the link between non-coherent and coherent symbol MAP detection of Continuous-Phase-Modulations. In preparation, 2018.

Table of Content

Adopted strategy

- Design simple and efficient serially concatenated coded CPM scheme in non-coherent regime
- Investigate classical existing system of transmission based on coded CPM scheme.
- Return channel of DVB-RCS2: CPM + convolutional code (CC)
- Evaluate its behaviour over non-coherent regime

Serially concatenated coded CPM scheme

- Carry on a joint iterative detection between the CPM demapper and a convolutional code (CC).
- EXIT charts analysis of both SISO components

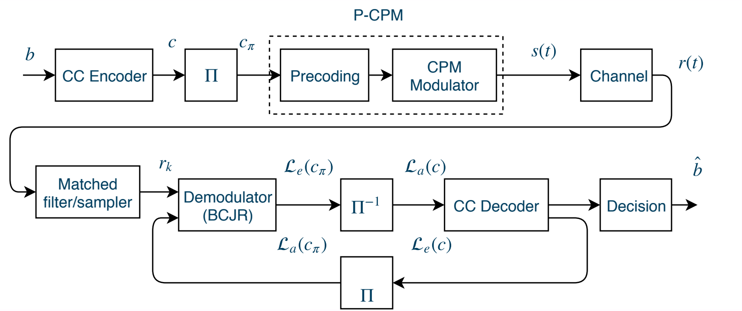

Figure: Coded interleaved CPM scheme with iterative decoding

Exit charts: quaternary 2RC

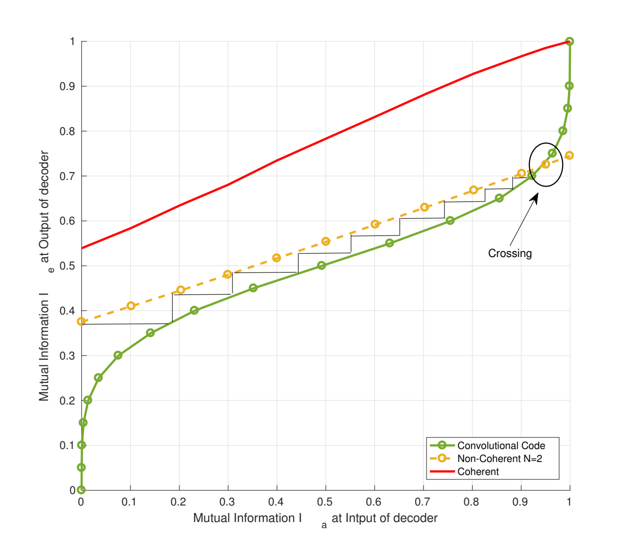

Figure: Exit charts: 2RC with $h = 1/4$, $M = 4$, $E_s/N_0 = 4.5\,dB$.

Finite length simulation

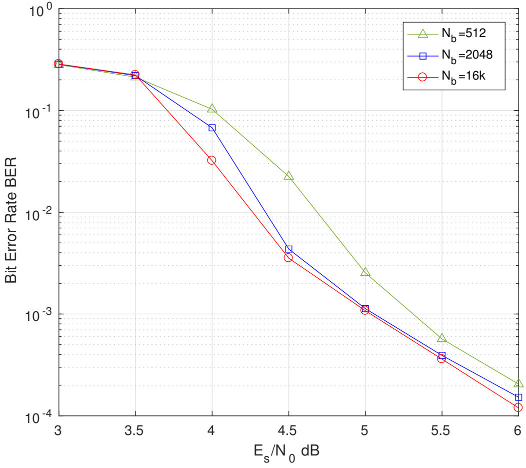

Figure: BER N.C. quaternary 2RC with $h = 1/4$ (natural mapping)

Open issues for serially concatenated coding scheme

- Classical approach:
  - Iterate between the CPM demodulator and the CC is not efficient in non-coherent regime
  - Due to EXIT charts convergence issue
- Issue
  - The detection procedure is blocked at a given iteration.
  - This interruption triggers an error floor
- Solution proposed
  - Design and optimize a precoding schemes which make the EXIT charts converge to the point (1,1) and unblocks the decoding process

Diagram of the non-coherent precoding

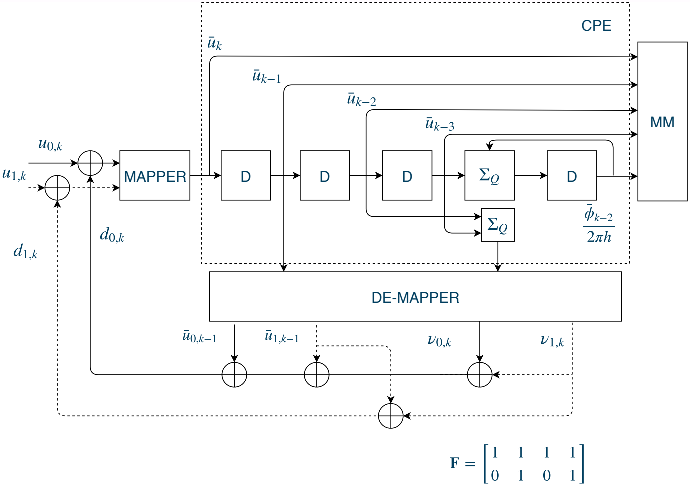

Figure: CPM modulator: quaternary CPM with $\mathbf{F} = [1\,3\,1\,3]$, $L = 2$ and $N = 3$

Modelization of the non-coherent precoding

- Precoded symbols:

$$\bar{u}_k = u_k \oplus d_k \tag{12}$$

- $\oplus$ is the sum over $\mathbb{Z}_2^m$,
- Precoded state : $\bar{\delta}_k = \{\bar{u}_{k-N-L+2}, \ldots, \bar{u}_{k-1}\}$
- The m bits of u_k are added modulo 2 to the m bits of d_k.

$$d_k = [\bar{u}_{k-1}, \ldots, \bar{u}_{k-L+1}, \boldsymbol{\nu_k}] \cdot \mathrm{F}^\top \tag{13}$$

- $\cdot$ is the matrix product and

$$\nu_k = \sum_{Q}{}_{i=k-N-L+2}^{k-L} \bar{u}_i \tag{14}$$

Modelization of the non-coherent precoding

- F is a $m \times r$-dimensional matrix whose components belong to $\mathbb{Z}_2$
- $r = m \cdot (L-1) + \lceil log_2(Q) \rceil$,
- $\lceil \cdot \rceil$ rounds to the next larger integer.
- $m = log_2(M)$
- $\boldsymbol{d}_k$ (respect. $\boldsymbol{\nu}_k$, $\boldsymbol{u}_k$) is the binary representation of d_k (respect. ν_k, u_k).
- $\sum_Q$ is the sum *modulo* Q.

Impact on the Exit charts

- Different EXIT charts trajectories
- Same Area under the curve.
- Same Information Rate.

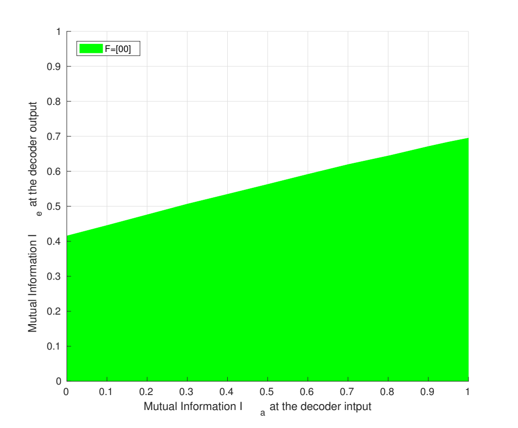

Figure: EXIT charts 1REC ($h = 0.25$ $M = 4$) for various F

Impact on the Exit charts

- Different EXIT charts trajectories
- Same Area under the curve.
- Same Information Rate.

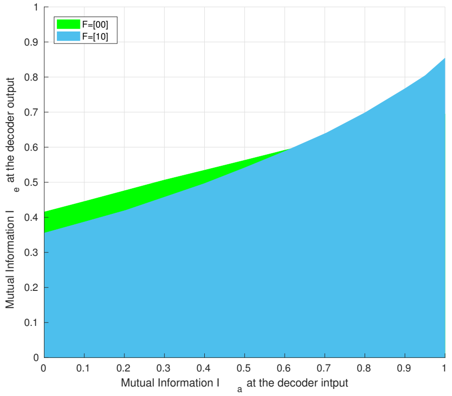

Figure: EXIT charts 1REC ($h = 0.25$ $M = 4$) for various F

Impact on the Exit charts

- Different EXIT charts trajectories
- Same Area under the curve.
- Same Information Rate.

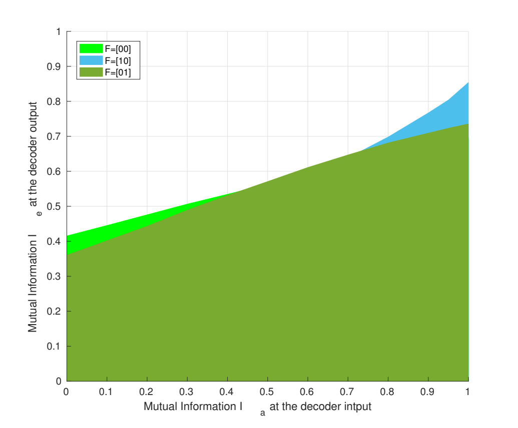

Figure: EXIT charts 1REC ($h = 0.25$ $M = 4$) for various F

Impact on the Exit charts

- Different EXIT charts trajectories
- Same Area under the curve.
- Same Information Rate.

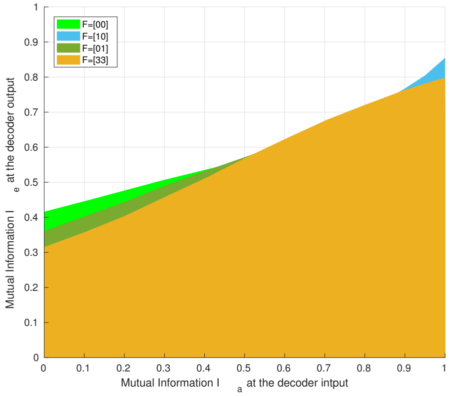

Figure: EXIT charts 1REC ($h = 0.25$ $M = 4$) for various F

Impact on the Exit charts

- Different EXIT charts trajectories
- Same Area under the curve.
- Same Information Rate.

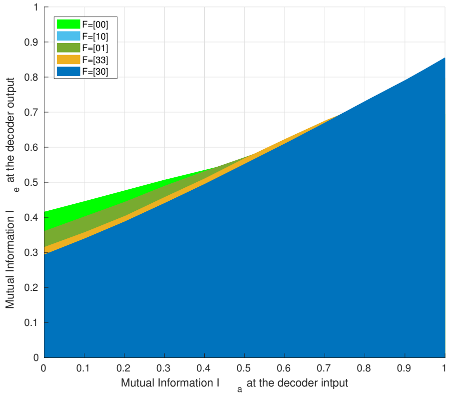

Figure: EXIT charts 1REC ($h = 0.25$ $M = 4$) for various F

Impact on the Exit charts

- Different EXIT charts trajectories
- Same Area under the curve.
- Same Information Rate.

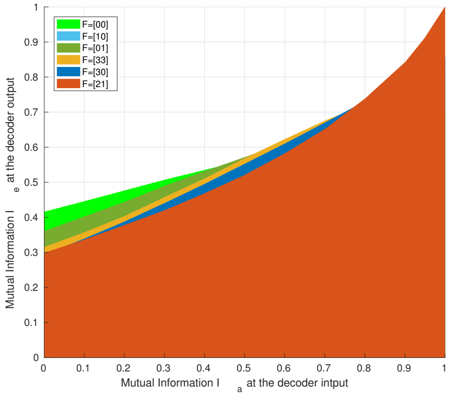

Figure: EXIT charts 1REC ($h = 0.25$ $M = 4$) for various F

Impact on the Exit charts

- Different EXIT charts trajectories
- Same Area under the curve.
- Same Information Rate.

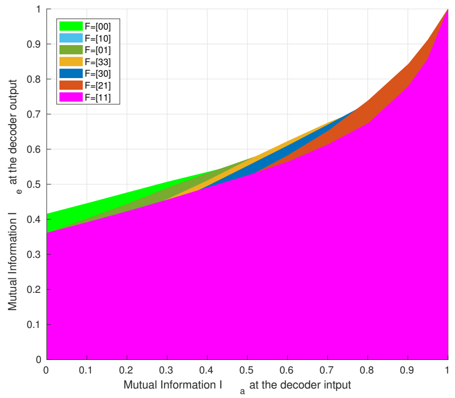

Figure: EXIT charts 1REC ($h = 0.25$ $M = 4$) for various F

Impact on the Exit charts

- Different EXIT charts trajectories
- Same Area under the curve.
- Same Information Rate.

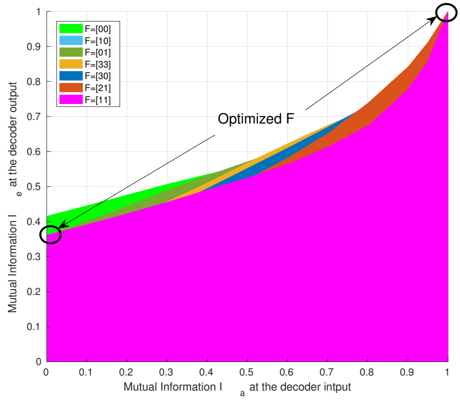

Figure: EXIT charts 1REC ($h = 0.25$ $M = 4$) for various F

Optimization procedure

- $\mathcal{F}$ the set of precoding $m \times r$-dimensional matrix F.
- $\text{card}(\mathcal{F}) = 2^{rm}$.
- $\mathcal{F}_c \subset \mathcal{F}$ the set of matrix enabling the convergence to point $(1,1)$.
- Select among $\mathcal{F}_c$ the one which generates the higher $I_e(0)$.

Exit charts analysis

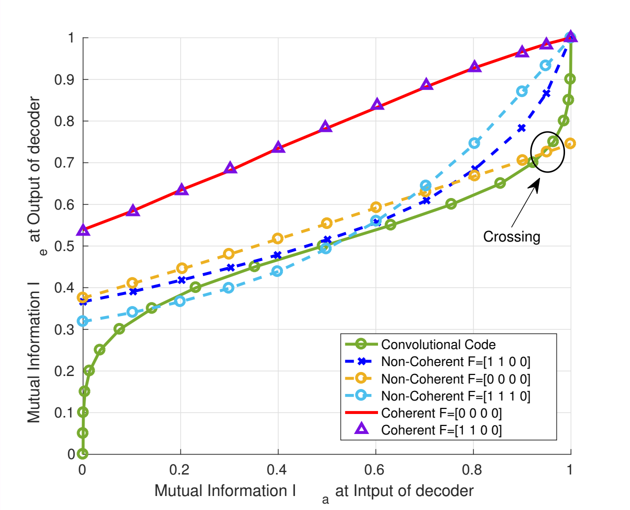

Figure: Exit charts quaternary 2RC with $h = 1/4$, $E_s/N_0 = 4.5\,dB$.

Finite length simulation

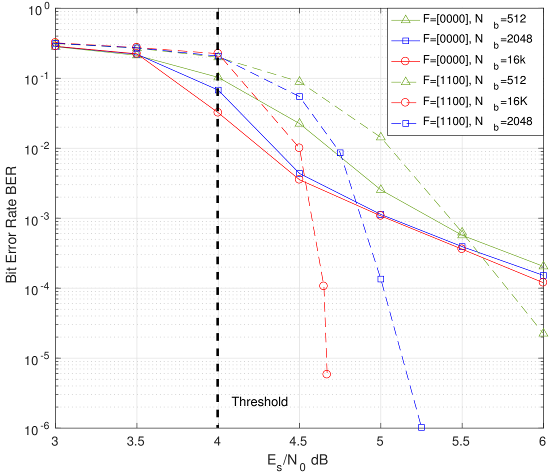

Figure: BER N.C. quaternary 2RC with $h = 1/4$ (natural mapping)

Contribution

Conference Paper: *Piat-Durozoi, C. U.*, Poulliat, C., Boucheret, M. L., Thomas, N., Bouisson, E., & Lesthievent, G. (2018, October). Precoding for Non-coherent detection of continuous phase modulations. MILCOM, 2018 in process, Los-Angeles California USA.

Journal paper: *Piat-Durozoi, C. U.*, Poulliat, C., Boucheret, M. L., Thomas, N., Bouisson, E., & Lesthievent, G. A novel nonbinary precoding for continuous phase modulations. To be submitted.

Table of Content

Open issues for capacity-achieving code

- Design capacity-achieving codes (sparse graph codes)
- Suited for both the coherent and non-coherent regimes
- Solution proposed
  - Consider LDPC coding scheme.
  - Optimization through EXIT chart analysis.

Serially concatenated coded CPM scheme

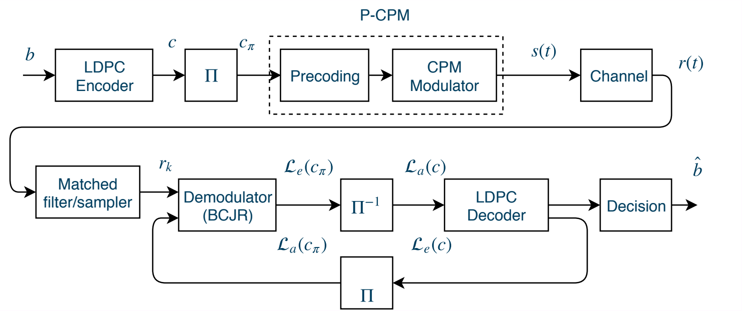

Figure: Coded interleaved CPM scheme with iterative decoding

LDPC codes

- Linear block codes
- Comprised of Variable Nodes (VN,λ,dv_{min},dv_{max}), Check Nodes (CN,ρ,dc_{min},dc_{max}) and edges

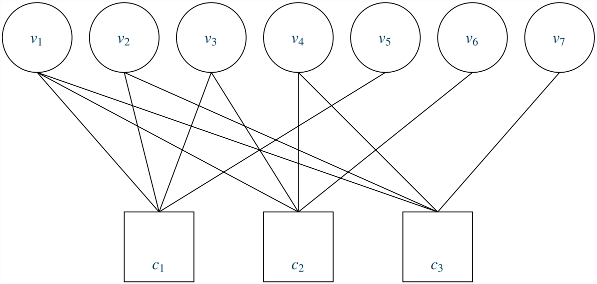

Figure: Tanner graph binary LDPC code

LDPC codes

- Low density of the parity matrix H

$$H = \begin{pmatrix} 1 & 1 & 1 & 0 & 1 & 0 & 0 \\ 1 & 0 & 1 & 1 & 0 & 1 & 0 \\ 1 & 1 & 0 & 1 & 0 & 0 & 1 \end{pmatrix} \quad (15)$$

- LDCP optimization principle: distribution NV, CN and edges

Serially concatenated CPM with irregular LDPC

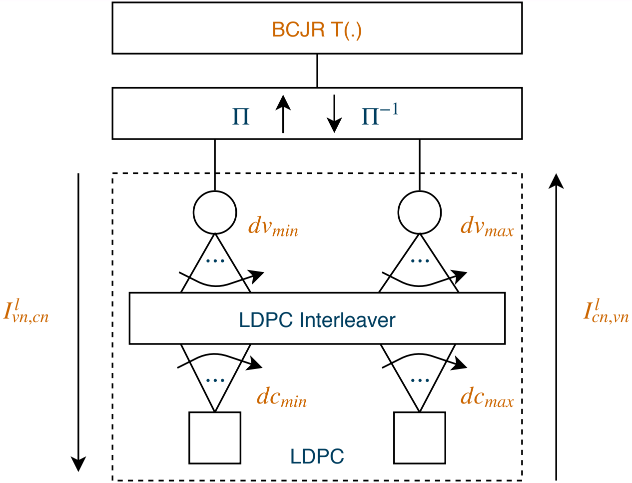

Figure: LDPC scheme

Optimization principles

- Maximize the rate

$$\mathcal{R} \geq 1 - \sum_{i=dc_{min}}^{dc_{max}} \frac{\rho_j}{j} / \sum_{i=dv_{min}}^{dv_{max}} \frac{\lambda_i}{i} \qquad (16)$$

- MI between VNs and CNs : $I_{vn,cn}^{l+1} = F(\lambda, T(.), I_{cn,vn}^{l})$
- Mixture constraint : $\sum_{dv_{min}}^{dv_{max}} \lambda_i = 1$
- Proportion constraint : $\lambda_i \in [0;1]$
- Convergence constraint : $I_{vn,cn}^{l+1} > I_{vn,cn}^{l}$
- Stability

condition : $\begin{cases} \text{d°1 :} \quad \lambda_1 < \frac{1}{T\prime(1)\sum \rho_j \cdot (j-1)} \; (T(1) = 1) \\ \text{d°2 :} \quad \lambda_2 < \frac{e^{[J^{-1}(T(1))]^2/8}}{\sum \rho_j \cdot (j-1)} \; (T(1) < 1) \end{cases}$

Code profiles optimization based on Exit charts

- Exit curves converge to point (1,1), then degree one VNs are allowed (Benaddi [Ben15]).
- Exit curves do not converge to point (1,1), then VNs are constrained in degree 2
- Coherent regime $dv_{min} => 1$ and Non-coherent regime $dv_{min} => 2$
- Issue:
  - A code suited to both regimes leads to LDPC profiles with $dv_{min} => 2$.

Code design algorithm (curve fitting)

- Fix a SNR
- Compute the CPM EXIT curve T(.) (polynomial approach)
- Fix dv_{max} and dv_{min}
- Initialize the code rate $\mathcal{R}_{opt} = 0$
- Fix ρ by generating a set $\mathcal{C}$ of concentrated CN profiles ρ
- For each ρ in $\mathcal{C}$ do
  - Solve linear programming and get the $\{\lambda_i\}$
  - Compute the new rate $\mathcal{R}$ from λ and ρ
  - If $\mathcal{R}_{opt} < \mathcal{R}$
    - $\mathcal{R}_{opt} = \mathcal{R}$, $\{\lambda_i\}_{opt} = \{\lambda_i\}$ and $\{\rho_i\}_{opt} = \{\rho_i\}$
  - End if
- End for

Parameters optimization

- Coherent VNs profile of Degree 2 > in NC regime
- Use the NC optimized coding schemes for both regime

Channel\Coding Optim.	C.	NC
C.	stable	stable
NC	unstable	stable

Table: Coding scheme stability

	d_c	d_v	ρ	λ
C.	$\{5,6\}$	$\{2,3,8\}$	$\{0.99, 0.01\}$	$\{0.4, 0.58, 0.02\}$
NC.	$\{5,6\}$	$\{2,3\}$	$\{0.04, 0.96\}$	$\{0.03, 0.97\}$

Table: Degree distribution from coding optim (2RC, $\mathcal{R} = 1/2$).

Asymptotic simulation

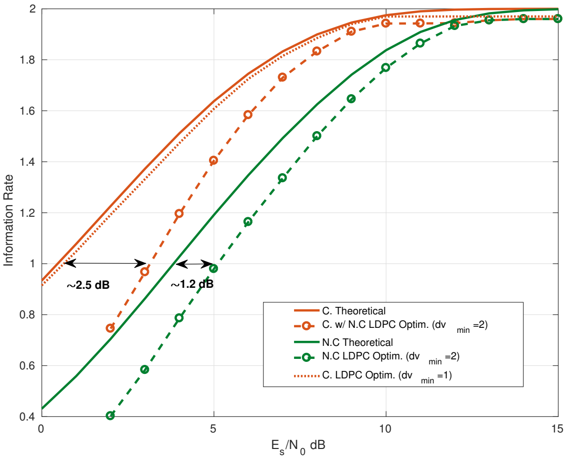

Figure: Information Rate: 2RC $h = 1/4$, $M = 4$

Optimization of precoded systems

- Issue:
  - Di□erential code profiles in both regimes
  - Degrees 2 variable nodes may generate a capacity penalty
  - Degrees 1 lead to better codes [Ben15]; [Ben+14].
- Solution proposed:
  - Optimized code profiles of precoded systems
  - Design code profile with degree 1
- Expected result:
  - Minimized the capacity penalty between the theoretical threshold and the optimized one

Exit chart analysis

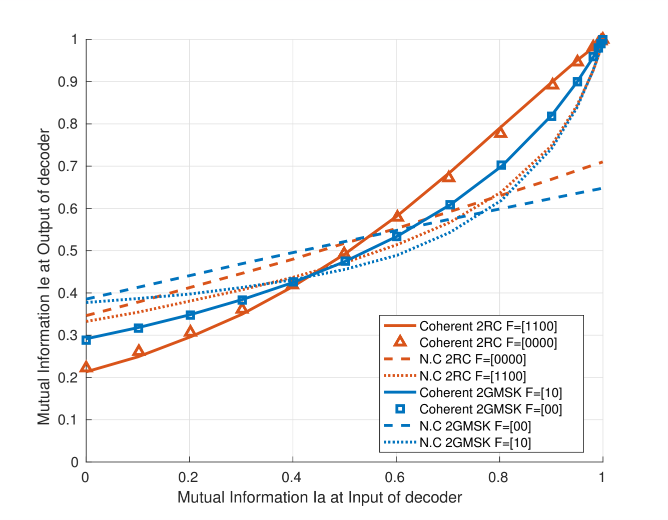

Figure: EXIT charts: 2GMSK $h = 1/2$, $M = 2$, $BT = 0.3$ and 2RC $h = 1/4$, $M = 4$

Parameters optimization

- Coherent VNs profile of Degree 1 > in NC regime
- Use the NC optimized coding schemes for both regime

Channel\Coding Optim.	C.	NC (w/ precoding)
C.	stable	stable
NC (w/ precoding)	unstable	stable

Table: Coding scheme stability

	d_c	d_v	ρ	λ
C.	$\{3,4\}$	$\{1,2,8\}$	$\{0.14, 0.86\}$	$\{0.26, 0.47, 0.27\}$
NC.	$\{4,5\}$	$\{1,2,8\}$	$\{0.04, 0.96\}$	$\{0.06, 0.6, 0.34\}$

Table: Degree distribution from coding optim (2RC, $\mathcal{R} = 1/2$).

Asymptotic simulation

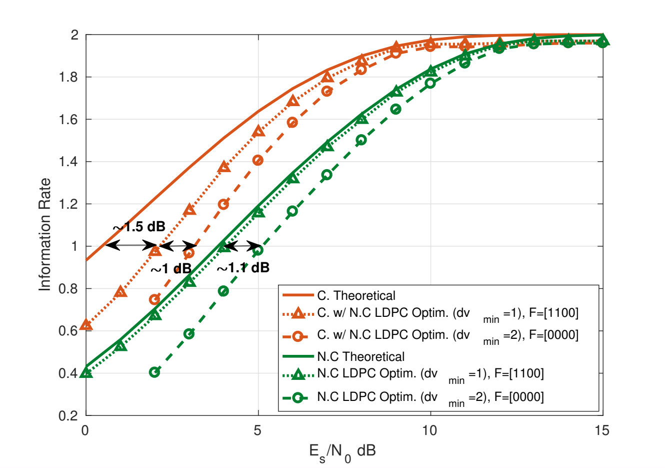

Figure: Information Rate: 2RC $h = 1/4$, $M = 4$

Contribution

Conference Paper: *Piat-Durozoi, C. U.*, Poulliat, C., Thomas, N., Boucheret, M. L., & Lesthievent, G. (2017, June). On sparse graph coding for coherent and noncoherent demodulation. In Information Theory (ISIT), 2017 IEEE International Symposium on (pp. 2905-2909). IEEE, Aachen Germany.

Journal: *Piat-Durozoi, C. U.*, Poulliat, C., Thomas, N., Boucheret, M. L., & Lesthievent, G. (2017, June). Precoding for non-coherent detection of continuous phase modulation. In preparation.

Table of Content

Conclusion

- Derivation of a non-coherent symbol/MAP receiver with minimal state space
- Design of non-coherent precoding enabling efficient iterative decoding between CPM and CC.
- Optimization of LDPC code profiles suited to both coherent and non-coherent regimes

Other contributions

- Non-binary precoding for low complexity coherent detection of coded CPM.
- Optimization of NB-LDPC for non-binary precoded system.
- Non-binary precoding for non-coherent detection of coded CPM (SICM).

Perspectives

- Protograph based solution for efficient coding scheme.
- Finite length simulation of the LDPC code optimization
- Extension to multi-h (adaptive rate)
- Channel estimation of the launcher's communication link
- Joint equalization and detection in non-coherent regime.

List of publications

- Journal paper
  - *Piat-Durozoi, C. U.*, Poulliat, C., Boucheret, M. L., Thomas, N., Bouisson, E., & Lesthievent, G. Reduced state non-coherent symbol MAP detection of Continuous-Phase-Modulations. IEEE Communication Letter, 2018.
  - *Piat-Durozoi, C. U.*, Poulliat, C., Boucheret, M. L., Thomas, N., Bouisson, E., & Lesthievent, G. A novel nonbinary precoding for continuous phase modulations. To be submitted.

List of publications

- International conference papers
  - *Piat-Durozoi, C. U.*, Poulliat, C., Thomas, N., Boucheret, M. L., & Lesthievent, G. (2017, June). Multisymbol with memory non-coherent detection of CPFSK. In Acoustics, Speech and Signal Processing (ICASSP), 2017 IEEE International Conference on (pp. 3794-3798). IEEE. New-Orleans USA.
  - *Piat-Durozoi, C. U.*, Poulliat, C., Boucheret, M. L., Thomas, N., Bouisson, E., & Lesthievent, G. (2017, March). On sparse graph coding for coherent and non-coherent demodulation. In Information Theory (ISIT), 2017 IEEE International Symposium on (pp. 2905-2909). IEEE, Aachen Germany.
  - *Piat-Durozoi, C. U.*, Poulliat, C., Boucheret, M. L., Thomas, N., Bouisson, E., & Lesthievent, G. (2018, October). Precoding for Non-coherent detection of continuous phase modulations. MILCOM, 2018 in process, Los-Angeles California USA.

List of publications

- National conference paper
  - *Piat-Durozoi, C. U.*, Poulliat, C., Thomas, N., Boucheret, M. L., Bouisson, E., & Lesthievent, G. (2017, Sept). Détection non-cohérente souple par bloc ou à mémoire des CPM. In Groupe de recherche sur le traitement du signal (GRETSI), Juan-Les-Pins France.

Other contributions

- Non-binary precoding for low complexity coherent detection of coded CPM.

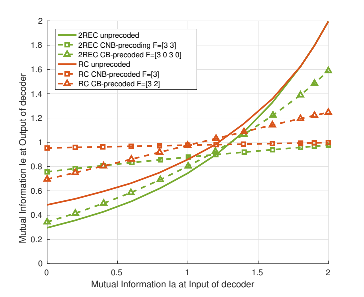

(a.)

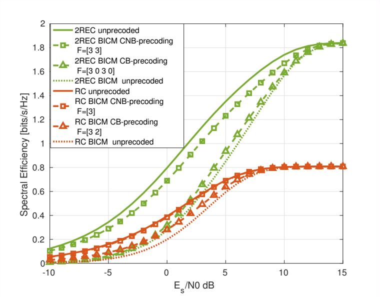

(b.)

Figure: 2REC $h = 1/4$, $M = 4$, RC $h = 1/4$ $M = 4$ (a.) Non-binary EXIT charts at $E_s/N_0 = 0\ dB$ (b.) Spectral E□ciency

Other contributions

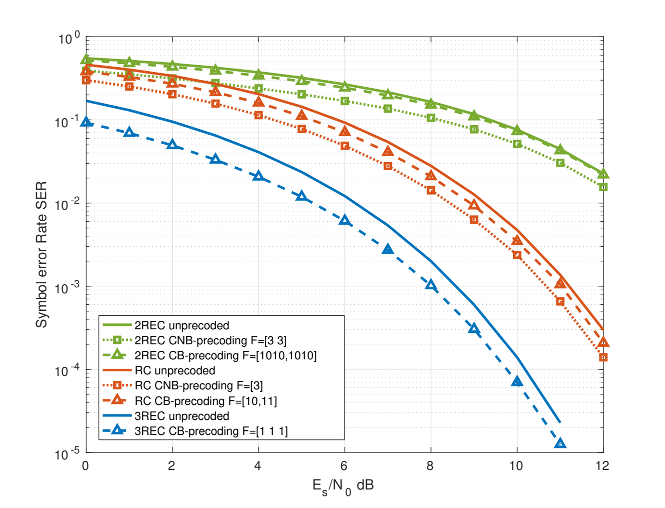

Figure: SER : 3REC $h = 1/2$ $M = 2$, 2REC $h = 1/4$, $M = 4$ and RC $h = 1/4$ $M = 4$

Other contributions

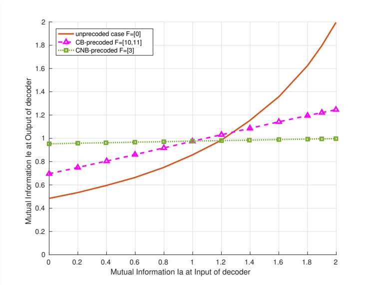

(a.)

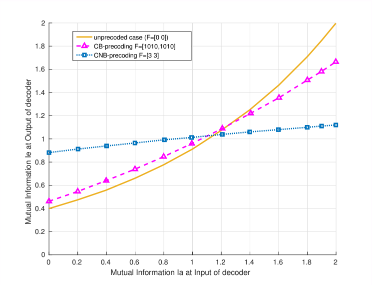

(b.)

Figure: Non-binary EXIT charts ($R = 1/2$) (a.) RC with $h = 1/4$ and $M = 4$ and (b.) 2REC with $h = 1/4$ and $M = 4$.

Other contributions

- Optimization of NB-LDPC for non-binary precoded system.

F	d_c	d_v	ρ	λ
2REC $(h = 1/4,\ M = 4)$				
[00]	$\{3,4\}$	$\{1,2,8\}$	$\{0.19,0.81\}$	$\{0.24,0.55,0.21\}$
RC $(h = 1/4,\ M = 4)$				
[0]	$\{3,4\}$	$\{1,2,8\}$	$\{0.69,0.31\}$	$\{0.12,0.63,0.25\}$
RC/2REC flat EXIT				
[3]/[33]	$\{5,6\}$	$\{2,3,8\}$	$\{0.59,0.41\}$	$\{0.33,0.32,0.35\}$

Table: Degree distribution NB-LDPC ($R = 1/2$).

Other contributions

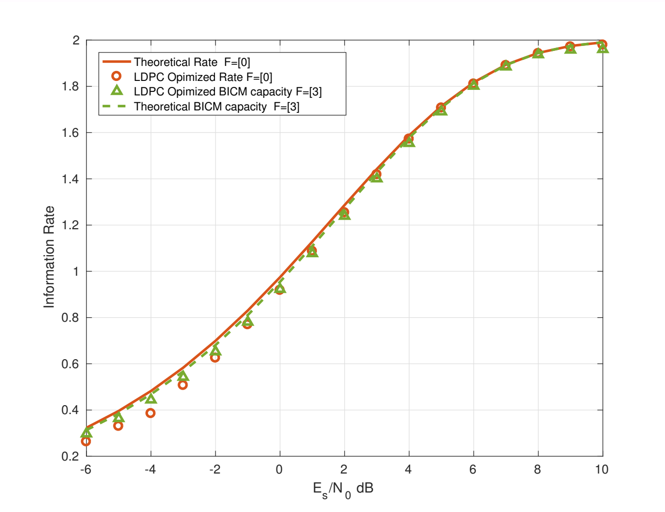

Figure: Information Rate ($R = 1/2$) (a.) RC with $h = 1/4$.

Other contributions

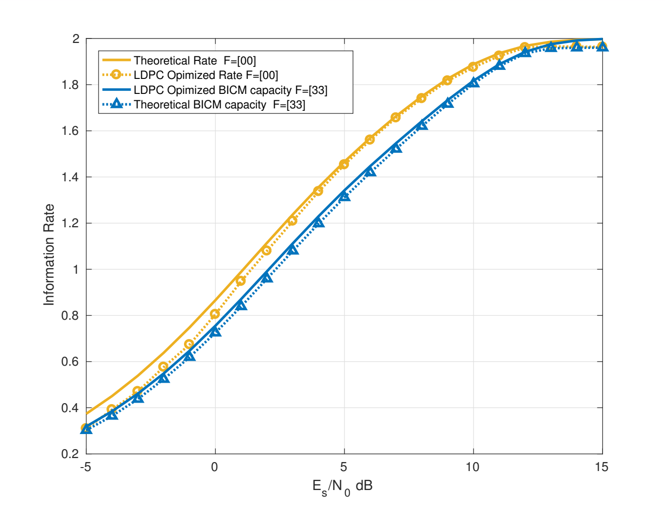

Figure: Information Rate 2REC with $h = 1/4$ and $M = 4$.

Réponse aux questions

- Complexité du récepteur par bloc: $8NM^{N+L-1} + 2M^{N+L} - M$
- Complexité du récepteur par treillis: $8NM^{N+L-1} + 2M^{N+L} \cdot \frac{4}{M} - M$

References I

John B Anderson, Tor Aulin, and Carl-Erik Sundberg. *Digital phase modulation*. Springer Science & Business Media, 2013 (cit. on p. 9).

Tarik Benaddi et al. "Design of unstructured and protograph-based ldpc coded continuous phase modulation". In: *Information Theory (ISIT), 2014 IEEE International Symposium on*. IEEE. 2014, pp. 1982–1986 (cit. on p. 63).

Tarik Benaddi. "Sparse graph-based coding schemes for continuous phase modulations". PhD thesis. 2015 (cit. on pp. 59, 63).

References II

Giulio Colavolpe, Gianluigi Ferrari, and Riccardo Raheli. "Noncoherent iterative (turbo) decoding". In: *IEEE Transactions on Communications* 48.9 (2000), pp. 1488–1498 (cit. on pp. 18, 22, 23, 30).

Dariush Divsalar and Marvin K Simon. "Multiple-symbol differential detection of MPSK". In: *IEEE Transactions on Communications* 38.3 (1990), pp. 300–308 (cit. on pp. 18, 22, 23).

Joachim Hagenauer. "The EXIT chart-introduction to extrinsic information transfer in iterative processing". In: *Signal Processing Conference, 2004 12th European*. IEEE. 2004, pp. 1541–1548 (cit. on p. 24).

John G Proakis. *Digital Communications Fourth Edition, Chapter 11, 2001*. (Cit. on p. 9).

References III

Dan Raphaeli and Dariush Divsalar. "Multiple-symbol noncoherent decoding of uncoded and convolutionally coded continuous phase modulation". In: *Journal of Communications and Networks* 1.4 (1999), pp. 238–248 (cit. on p. 18).

Bixio E Rimoldi. "A decomposition approach to CPM". In: *IEEE Transactions on Information Theory* 34.2 (1988), pp. 260–270 (cit. on p. 18).

DVB Second Generation. "Digital Video Broadcasting (DVB); Second Generation DVB Interactive Satellite System". In: (2013) (cit. on p. 27).

References IV

Stephan Ten Brink. "Convergence behavior of iteratively decoded parallel concatenated codes". In: *IEEE transactions on communications* 49.10 (2001), pp. 1727–1737 (cit. on p. 24).

Matthew C Valenti, Shi Cheng, and Don Torrieri. "Iterative multisymbol noncoherent reception of coded CPFSK". In: *IEEE transactions on communications* 58.7 (2010), pp. 2046–2054 (cit. on p. 18).